A. Celletti, C. Froeschlé, I. V. Tetko, and A. E. P. Villa. Determination of chaotic attractors in short discrete time series. In B. A. Steves and A. J. Maciejewski, editors, *The Restless Universe: Applications of Gravitational N-Body Dynamics to Planetary Stellar and Galactic Systems*, Chapter 18, pages 339–360. Institute of Physics Publishing, Bristol, UK, 2001.

Determination of chaotic attractors in short discrete time series

A Celletti[1], C Froeschlé[2], I V Tetko[3], A E P Villa[4]

[1]Universitá di Roma, [2]Observatoire de Nice, [3]Academy of Sciences of Ukraine, [4]Université de Lausanne.

1 Introduction

Discrete time series can represent the occurrences of either a deterministic or a random process. Dynamical system theory provides powerful techniques to assess whether a set of equations (in a suitable embedding space) underlies the dynamics. In this case the trajectory can be predicted whenever the initial conditions are known with absolute precision. On the contrary, a stochastic system is characterised by a complete unpredictability of the trajectories. Time series may be derived from mathematical models, either from mappings or from continuous models. The time series may be also provided by experimental data, derived, e.g., from astronomy, physics, medicine and biology. In particular, we present an analysis of neuro-biological data, where the discrete time series are obtained from the epochs of action potentials of nervous cells (i.e., *spike trains*). We refer to Babloyantz and Salazar (1985), Celletti and Villa (1996), Mpitsos *et al.* (1988), Rapp *et al.* (1985) for extensive applications of dynamical system methods to neurobiology.

In recent years several techniques have been extensively developed to determine the deterministic or stochastic behaviour of a time series (Abarbanel *et al.* 1993, Boffetta *et al.* 1998, Celletti *et al.* 1999, Cellucci *et al.* 1997, Gao and Zheng 1993, Eckmann and Ruelle 1985, Kaplan and Glass 1992, Rapp *et al.* 1993, Sugihara and May 1990, Theiler *et al.* 1992). An exhaustive description of methods in nonlinear time series analysis is presented in Hegger *et al.* (1999), Schreiber (1998). Beside the characterisation of the embedding space, topological and metric invariants can be determined. On the one hand, the method developed by Grassberger and Procaccia (1983) allows computation of the size of the attractor, i.e. the so-called *correlation dimension*. On the other hand, the computation of Lyapunov exponents quantifies the divergence of nearby trajectories, providing an analysis of the structure of the attractor (Dämming and Mitschke 1993, Eckmann *et al.* 1986, Kantz 1994, Packard *et al.* 1980, Rosenstein *et al.* 1993, Wolf *et al.*

1985, Zeng *et al.* 1991). We devote Section 2 to the definitions of fractal dimensions; a review of the Grassberger and Procaccia method and of the basic techniques to compute Lypaunov exponents is presented in Sections 3 and 4, respectively.

A common hindrance of most methods is a severe constraint due to the necessity of having a *sufficiently large* number of points in the time series in order to avoid unreliable results due to poor statistics. During physical experiments long observations may be corrupted by drifts and non stationarities which may lead to incorrect results. Therefore, the availability of *long* time series can be a serious limitation in the investigation of nonlinear dynamics in physical systems. We stress that the statistics required by standard investigation methods usually prevents the applicability of the algorithms in realistic situations. The development of methods able to distinguish the deterministic character of *short* time series becomes an important issue for future research in this field.

A *new* method to provide information on the deterministic properties of time series $\{x_i\}$, $i = 1, ...K$, with a significant but not too large number of points was presented in Celletti *et al.* (1999). In particular, this algorithm was applied to the 2–dimensional Hénon mapping taking $K = 400$ and to the Rössler system with $K = 1000$. In Section 5 we explore in more detail the method presented in Celletti *et al.* (1999), providing a large variety of applications to discrete and continuous systems, as well as to surrogate data (see Section 6). We provide also a validation for the choice of the parameters on which the method depends. Among the mathematical models we have investigated, we selected the mappings known as Hénon (and its extension in 4 dimensions), Kaplan–Yorke, Zaslavskii, Ikeda, Sinai and the continuous systems known as Lorenz, Rössler and the hyperchaotic Rössler attractor. The time series were constructed as the iterates of one variable with only $K = 1000$ points. In all cases the deterministic behaviour of the system was correctly detected. Moreover, we use the method presented in Celletti *et al.* (1999) to give an estimate of the maximum Lyapunov exponent (or *Lyapunov characteristic estimate*, hereafter LCE). We perform a comparison of the LCE with the classical numerical expectations. In order to explore the robustness of the method, we analyse the effect of additive, dynamical and experimental noise. The stochastic behaviour is already observed with noise levels of 5%. The results suggest a much higher sensitivity of our method with comparison to other algorithms, such as the Grassberger and Procaccia. As a further check, we test the method on several sets of surrogate data and we always observe a stochastic behaviour.

A question was left open in Celletti *et al.* (1999), namely the effectiveness of the method when applied to realistic situations. To this end, we consider in Section 6 experimental time series derived from electro-physiological recordings of neuronal discharges in the cerebral cortex of anaesthetised mice and in the red nucleus of behaving rats. Although the majority of these experimental data show a stochastic behaviour, some cases reveal a deterministic behaviour in low–dimensional spaces.

The method presented in Section 5 does not provide reliable results in some specific cases of symplectic mappings (precisely, regular motions and weak chaos). In Lega *et al.*, (2000) alternative methods based on the technique of Section 5 have been developed to deal with such degenerate cases. The most promising algorithm is briefly summarised in Section 7. The conclusions are discussed in Section 8.

A practical implementation of many algorithms from time series analysis can be found in `http://www.neuroheuristic.org` where a *virtual laboratory* is installed.

2 Fractal dimensions

Given a set of points, fractal dimensions are related to the way the density of points scales with small volumes surrounding the points (Abarbanel, 1996). The simplest way to assign a fractal dimension is obtained by a *box-counting* method. Sets with noninteger dimension are called *fractals.* To introduce the box-counting dimension, consider a set in an N-dimensional space, which we cover by a grid of N-dimensional cubes of side r. Let $\widetilde{N}(r)$ be the number of cubes which are needed to cover the set. The box-counting dimension is defined as

$$D_0 = \lim_{r\to 0} \frac{\log \widetilde{N}(r)}{\log\left(\frac{1}{r}\right)} .$$

As an example, we consider the middle third Cantor set. To compute its box-counting dimension, we define a sequence r_n with the property that $\lim_{n\to\infty} r_n = 0$. Then D_0 can be rewritten as

$$D_0 = \lim_{n\to\infty} \frac{\log \widetilde{N}(r_n)}{\log\left(\frac{1}{r_n}\right)}$$

In particular, one can take $r_n = 1/3^n$, so that $\widetilde{N}(r_n) = 2^n$ and $D_0 = \log 2/\log 3 \simeq 0.63$, providing the fractal property of the Cantor set.

As an extension of the box-counting dimension, one defines the following family of *generalised dimensions,* which depend on an index q:

$$D_q = \frac{1}{1-q} \lim_{r\to 0} \frac{\log I(q,r)}{\log\left(\frac{1}{r}\right)} ,$$

where $I(q,r) \equiv \sum_{i=1}^{\widetilde{N}(r)} \mu_i^q$ and the sum is over all $\widetilde{N}(r)$ cubes of unit size r which are needed to cover the attractor. The quantities μ_i are the *natural measure* of the attractor. More precisely, if the attractor is covered by a grid of cubes C_i, for any x_0 in the basin of attraction, let us define

$$\mu_i = \lim_{T\to\infty} \frac{\eta(C_i, x_0, T)}{T} ,$$

where $\eta(C_i, x_0, T)$ is the time spent in C_i by the orbit starting from x_0 for any $0 \le t \le T$.

For $q = 1$ one has the *information dimension* D_1: let the attractor be covered by $\widetilde{N}(r)$ cubes of size r and let p_i be the probability to visit the i-th cube. Then D_1 is defined as

$$D_1 = \lim_{r\to 0} \frac{-\sum_{i=1}^{\widetilde{N}(r)} p_i \log p_i}{|\log r|} .$$

For $q = 2$, one obtains the *correlation dimension* D_2 which will be introduced in the following section, being at the basis of the Grassberger and Procaccia method.

3 The method of Grassberger and Procaccia

A basic problem when dealing with discrete time series is to ascertain whether the series is produced by a deterministic or stochastic system. In the first case, one assumes there exists a set of equations governing the dynamics in a suitable embedding space. In the latter case, due to the randomness of stochastic motion, no forecasting can exist on the dynamics. Among several methods available for classification of discrete time series the algorithm of Grassberger and Procaccia (1983), hereafter referred to as GP method, has been widely applied to theoretical and experimental cases. If the observable is deterministic the GP method enables to determination of the dimensions of the embedding space and of the attractor. We briefly recall the method as follows. Let $\{x_1, ..., x_K\}$ ($x_j \in \mathbf{R}$) be a discrete time series composed by K points. In a d-dimensional embedding space, define the set $Y \equiv \{y_1, ..., y_N\}$ ($N = K - d + 1$) of *delay* vectors as

$$\begin{aligned} y_1 &= (x_1, ..., x_d) \\ y_2 &= (x_2, ..., x_{d+1}) \\ &\dots \\ y_N &= (x_N, ..., x_K) . \end{aligned}$$

Let $r > 0$ and for any $y_j \in Y$, let $n_j(r; d)$ be the number of points $y_i \in \mathbf{R}^d$ ($i \neq j$) which are contained in the d-dimensional hypersphere of radius r around y_j, i.e.

$$n_j(r; d) = \sum_{i=1, i\neq j}^{N} \Theta(r - \|y_i - y_j\|_d) ,$$

where Θ is the Heaviside function (*i.e.* $\Theta(x)=1$ for $x \geq 0$, $\Theta(x)=0$ for $x<0$) and $\|\cdot\|_d$ is the Euclidean norm in $\mathbf{R}^d$. We define the *correlation integral* functions as

$$C_{N,d}(r) \equiv \frac{1}{N^2} \sum_{j=1}^{N} n_j(r; d) .$$

The *correlation dimension* D_2 is related to $C_{N,d}(r)$ by

$$D_2 \equiv \lim_{r\to 0} \lim_{N\to\infty} \frac{\log C_{N,d}(r)}{\log r} ,$$

for d sufficiently large. We remark that the correlation dimension corresponds to the generalised dimension of order $q = 2$, since it can be shown that $C_{N,d}(r)$ scales as $I(2, r)$. Moreover, one has the inequalities $D_2 \leq D_1 \leq D_0$; if the points on the attractor are uniformly distributed, then $D_2 = D_1 = D_0$. The correlation dimension corresponds to the slope of the graph $\log C_{N,d}(r)$ against $\log r$, whenever its value is nearly constant as the embedding dimension d is varied (see Figure 1a). This algorithm enables computation of the correlation dimension as well as the dimension of the embedding space, provided that the slopes of the above curves are definitely convergent. A stochastic behaviour is given by a constant increase of the slopes with d (see Figure 1b).

In practical applications, the slope of the curves $\log C_{N,d}(r)$ against $\log r$ must be evaluated in a meaningful range of values of the radius, say (r_0, r_1), denoted as the *scaling region*. Below r_0 the curves are distorted since few points are counted in the hypersphere of radius r_0, while above r_1 the curves tend to flatten since the attractor has finite size. The relation between the minimum amplitude of the scaling region and the number of points forming the time series was investigated in Eckmann and Ruelle, (1992). An extension of the Grassberger and Procaccia method to analyse the joint behaviour of two (or more) time series was investigated in Celletti *et al.* (1998).

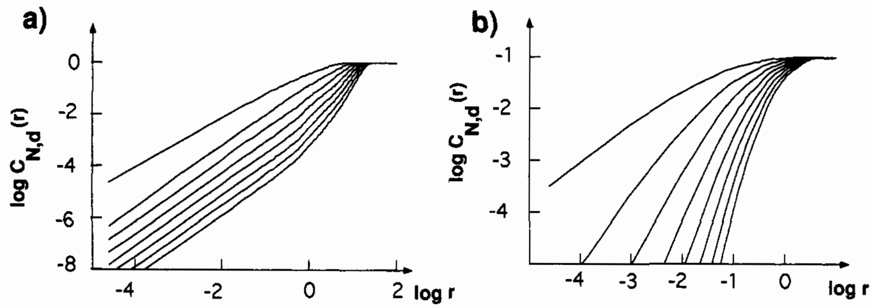

Figure 1. *Graphs of* $\log C_{N,d}(r)$ *against* $\log r$ *for embedding dimensions* $d = 1, ..., 8$*: (a) the deterministic behaviour is indicated by the parallelism of the curves from* $d = 2$*; (b) the stochastic character is determined by the divergence of the slopes of the correlation integral curves.*

4 Lyapunov exponents

The calculation of the Lyapunov exponents (Benettin and Galgani 1979, Benettin *et al.* 1980, Dämming and Mitschke 1993, Eckmann *et al.* 1986, Kantz 1994, Packard *et al.* 1980, Rosenstein *et al.* 1993, Wolf *et al.* 1985, Zeng *et al.* 1991) provides information on the evolution of the motion and, more precisely, the rate of divergence of nearby orbits.

Most methods for determining the Lyapunov exponents are based on the following idea introduced in Benettin and Galgani (1979), Benettin *et al.* (1980). Compute the spectrum of the Lyapunov exponents following the evolution of a set of tangential vectors, which might be approximated by small distance vectors. A renormalisation procedure is applied at given intervals of time in order to control the overflow of chaotic orbits. More precisely, consider two orbits starting at P_0 and P_0' with $\mathrm{dist}(P_0, P_0') = d_0$ (Figure 2).

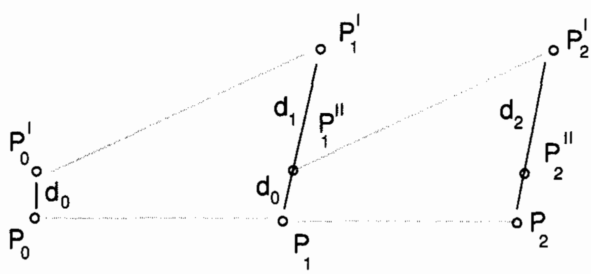

Figure 2. *The Benettin and Galgani method (see Benettin and Galgani, 1979).*

After a time h, P_0 evolves into P_1 and P_0' into P_1' with $\mathrm{dist}(P_1, P_1') = d_1$. By a homothesis of the centre P_1 and of the ratio d_0/d_1, one finds a new point P_1'' at distance d_0 from P_1. Iterating this process (with new initial data P_1, P_1'') one obtains a sequence of points at distances d_1, d_2, d_3,... The quantity:

$$\gamma(P_0, n, d_0, h) = \frac{1}{n} \sum_{i=1}^{[n/h]} \log \left(\frac{d_i}{d_0} \right)$$

tends to a limit, which is the largest Lyapunov characteristic estimate as the number n tends to infinity and as the distance d_0 tends to zero. We remark that in order to apply the above method, it is essential to know the explicit equations governing the dynamics. However, the previous technique can be adapted to investigate discrete time series as described in Wolf *et al.* (1985). More precisely, follow the evolution of two points P_0, P_0', until their distance exceeds a given value, (Figure 3). Let P_1, P_1' be the evolved points; replace P_1' with a point P_1'' closer to P_1 and such that the vector P_1P_1'' has the same orientation as P_1P_1'. Let $\{t_k\}$ be the sequence of times at which the replacements take place and let $d(t_k)$ =dist(P_k, P_k'), $d'(t_k)$ =dist(P_k, P_k''). The largest Lyapunov exponent is defined as

$$L_1 = \frac{1}{t_n - t_0} \sum_{k=1}^{n} \log \frac{d(t_k)}{d'(t_{k-1})} ,$$

where n is the total number of replacements.

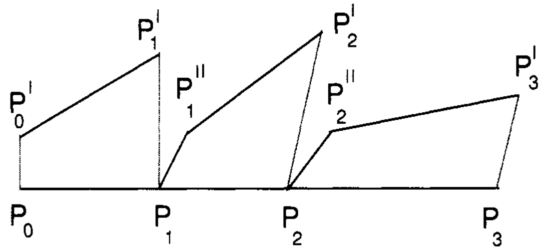

Figure 3. *The Wolf et al. method (see Wolf et al., 1985).*

An alternative method to compute the whole spectrum of the Lyapunov exponents was developed in Eckmann *et al.* (1986). Suppose that the dynamics is ruled by

$$x_{n+1} = f(x_n)$$

and let $D_{x_n} \equiv \left(\frac{\partial f}{\partial x_j}\right)_{x_n}$. We look for an approximation of D_{x_n} using the experimental data as follows. Consider the evolution of the points P_i', whose distance from a preassigned point P_i is less than r, (Figure 4). Consider those points whose images P_{i+m}' are still at distances less than r from P_{i+m}. Determine D_{x_n} with a least square approximation over the points P_i', so that

$$D_{x_n}[P_i' - P_i] \simeq P_{i+m}' - P_{i+m} .$$

Determine the matrices $D_{x_{i+m}}$, $D_{x_{i+2m}}$, ... in the same way. Next, let us decompose the matrix D_{x_1} as $D_{x_1} = Q_1R_1$, where Q_1 is an orthogonal matrix, while R_1 is an upper triangular matrix with non-zero diagonal elements. Analogously, let $D_{x_{1+m}}Q_1 = Q_2R_2$, ..., $D_{x_{1+nm}}Q_n = Q_{n+1}R_{n+1}$. The Lyapunov exponents are given by the formula

$$L_k = \frac{1}{\tau m M} \sum_{j=1}^{M-1} \log(R_j)_{kk} , \qquad L_k > L_{k+1} ,$$

where τ is the sampling time step, $(R_j)_{kk}$ is the k-th diagonal element of R_j and M is the available number of matrices.

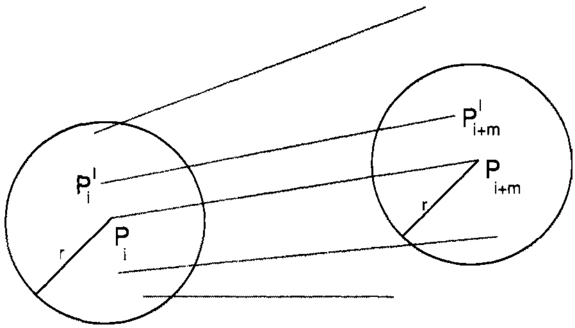

Figure 4. *The Eckmann et al. method (see Eckmann et al., 1986).*

5 A method for short time series

The main drawback of the methods for computing Lyapunov exponents and correlation dimensions consists in the large number of points required to avoid inaccuracy and errors during the calculation. A careful analysis of the minimal number of points necessary to compute correlation dimension and Lyapunov exponents has been presented in Eckmann and Ruelle (1992). In addition, the calculation of the methods presented in Sections 3 and 4 often relies on the choice of some parameters, which are not easily selected. In this section, we review the method presented in Celletti *et al.*, (1999) to assess the deterministic character of short time series (typically composed by 1000 points), providing more details for the criterion of selection of the parameters on which the method depends.

Let $\{x_l\}$, $l = 1, ..., K$, be a discrete time series with K points. We then consider delay coordinates in a d-dimensional embedding space, setting $y_j = (x_j, ..., x_{j+d-1})$ for $j = 1, ..., K - d + 1$. Denote by $P_j \equiv (y_j)$ a point in the embedding space and let $P_j^{(k)} = (y_{j+k})$ be the k-th iterate of P_j. For $r_0 > 0$, let $n(r_0)$ be the number of pairs (P_i, P_j), $i < j$, such that $d_{ij}^{(0)} \equiv \|P_i - P_j\|_d \leq r_0$. We denote by $d_{ij}^{(k)} \equiv \|P_i^{(k)} - P_j^{(k)}\|_d$ the distance between the k-th iterates of P_i, P_j. Let $\alpha_{ij}^{(k)} \equiv \log(d_{ij}^{(k)}/d_{ij}^{(0)})$ and let

$$\lambda_k(r_0) \equiv \frac{1}{n(r_0)} \sum_{\{i,j:d_{ij}^{(0)} \leq r_0\}} \alpha_{ij}^{(k)} = \frac{1}{n(r_0)} \sum_{\{i,j:d_{ij}^{(0)} \leq r_0\}} \log \frac{d_{ij}^{(k)}}{d_{ij}^{(0)}} . \tag{1}$$

We refer to $\lambda_1(r_0)$ as the *Lyapunov characteristic estimate* (LCE). An estimate of the LCE can be equivalently obtained as $\lambda_k(r_0)/k$. We may therefore set the following criteria:

1. In a low-dimensional deterministic system, there exists a suitable interval of initial distances r_0 in which, for a fixed k, the value of the LCE is nearly constant; the curves $\lambda_k(r_0)$ against r_0 tend to become parallel because the values $\lambda_k(r_0)/k$ are nearly equal as k is varied.

2. In stochastic or higher dimensional deterministic systems, the value of the LCE, for a fixed k, decreases with r_0, due to the unpredictability character of stochastic dynamics; the curves $\lambda_k(r_0)$ against r_0 tend to converge to the same limit.

Note that the above criteria depends only on two parameters: the iteration parameter k and the initial distance r_0. The value of the largest LCE is given by $\lambda_1(r_0)$ when it is nearly constant with the initial distance r_0.

Remark: The measure at the basis of our method (i.e., the quantity $\lambda_k(r_0)$) was introduced in other studies (Boffetta *et al.* 1998, Cellucci *et al.* 1997, Gao and Zheng 1993, Kantz 1994), though the analysis of *short* time series (like those studied in the present section) was not performed and simple criteria for applicability to real situations were not discussed. In particular, Gao and Zheng (1993) proposed a *local exponential divergence plot* aimed at determining the minimal embedding dimension. An algorithm to detect noise corruption was presented by Cellucci *et al.* (1997). A measure similar to LCE has been suggested to compute Lyapunov exponents for dynamical systems characterised by different time scales (Boffetta *et al.* 1998). The dependence of the LCE upon noise was investigated in Dämming and Mitschke (1993).

5.1 Choice of the iteration parameter

A variation of the iteration parameter k implies a comparison of the initial distance $d_{ij}^{(0)}$ of some pairs of points, say P_i and P_j, with the distance $d_{ij}^{(k)}$ after k iterations of the above points. In order to keep control of the divergence of the corresponding trajectories, it is essential to take a reasonable low value of the iteration parameter, since in a deterministic chaotic system the trajectories diverge exponentially. It is rational to consider a maximum number of $k = 5$ iterations as sufficient to control the separation of the orbits.

5.2 Choice of the initial distance

As mentioned in Celletti *et al.* (1999), the value of the initial distance is crucial for the statistics of our method: for a small value of r_0, the number of pairs within r_0 is generally too small to provide meaningful results. On the contrary, if r_0 is too large all points of the embedding space will be included, eventually exceeding the actual size of the attractor, if any. If K denotes the number of points which form the time series, we have heuristically determined to select an optimal value $r_{\max}$ for the distance r_0 such that $n(r_{\max}) = K^2/100$, where $n(r_{\max})$ is the number of pairs (P_i, P_j), $i < j$, whose distance is less than or equal to $r_{\max}$. The validation of this 'rule of the thumb' has been performed by a χ^2 comparison of the distribution of the $\lambda_1(r_{\max})$ with the *classical numerical* result, when dealing with explicitly known dynamical systems. The rationale is that for optimal values of r_0 the LCE-curves are flat parallel lines and in the case of low-dimensional systems the value of the estimated LCE is nearly constant on this plateau. The classical numerical estimate of the LCE is performed as follows (Froeschlé, 1984): let $M : \mathbf{R}^d \to \mathbf{R}^d$ be a mapping in a d-dimensional embedding space. We derive the tangent mapping at a point $x_0 \in \mathbf{R}^d$, say $DM(x_0)$, and for a given initial vector $v_0 \in \mathbf{R}^d$ we compute the image point as $v_1 = DM(x_0)v_0$. After normalising the sequence of vectors, the greater LCE is given by

$$\lambda_C \equiv \frac{1}{N_0} \sum_{i=1}^{N_0} \log \frac{||v_{i+1}||_d}{||v_i||_d} , \tag{2}$$

where N_0 is a suitable number of iterations at which convergence is reached.

A χ^2-test is performed between the LCE computed as in (2) and as in (1) with $k = 1$. More precisely, let $[a, b)$ be an interval in $\mathbf{R}$; consider a pairwise disjoint partition of $[a, b)$, say $[a, b) \equiv \cup_{l=1}^{n}[a_l, b_l)$ for a suitable $n > 1$. For a given r_0, we denote by $\Pi_1([a_l, b_l))$ the number of values $\alpha_{ij}^{(1)}$, $i = 1, ..., K-1$, $j = i+1, ..., K$, belonging to the interval $[a_l, b_l)$. Using the same notation, $\Pi_2([a_l, b_l))$ is the number of values $\log \frac{\|v_{i+1}\|_d}{\|v_i\|_d}$, $i = 1, ..., N_0$, which fall in the interval $[a_l, b_l)$.

The standard χ^2-value is provided by

$$\chi^2(r_0) \equiv \sum_{l=1}^{n}[\Pi_1([a_l, b_l)) - \Pi_2([a_l, b_l))]^2 .$$

Notice that the quantities $\alpha_{ij}^{(1)}$ and henceforth $\Pi_1([a_l, b_l))$ depend on r_0. The value r_{optimal} at which χ^2 as a function of r_0 reaches its minimum is the optimal initial distance at which the LCE computed as $\lambda_1(r_0)$ (see (1)) is the nearest to the *classical numerical* value.

The validation by this test was performed on well known low-dimensional mathematical models, the Hénon and the Sinai mappings (see also section 6). In Figure 5 we illustrate the corresponding χ^2-functions. Note that r_{optimal} determined as the minimum of the χ^2-function nearly coincides with $r_{\max}$ such that $n(r_{\max}) = K^2/100$: for the Hénon case, taking $K = 1000$ we have $r_{\text{optimal}} \simeq 0.02$, $r_{\max} \simeq 0.014$, while for the Sinai map we have $r_{\text{optimal}} \simeq 0.067$, $r_{\max} \simeq 0.064$.

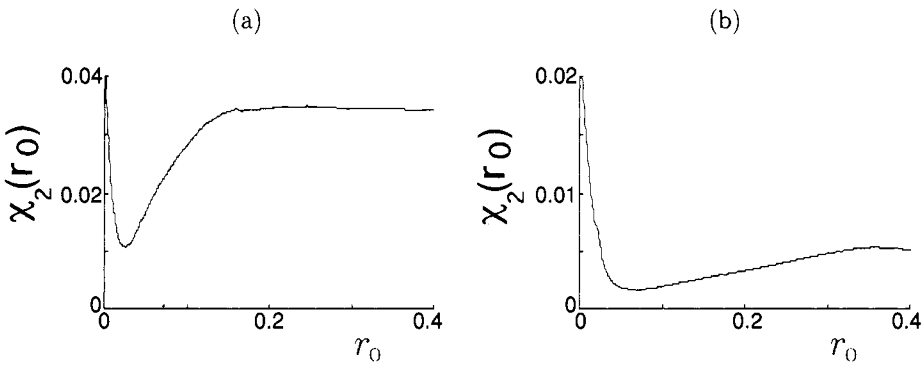

Figure 5. *The curves $\chi^2(r_0)$ against r_0 are displayed for: (a) The Hénon mapping with initial data $x_0 = 0.6$, $y_0 = 0.19$ and for the parameters: $a = 1.6$, $b = 0.1$ $(d = 2)$; (b) The Sinai mapping with $x_0 = 0.1$, $y_0 = 0.1$ and $\Delta = 0.1$ $(d = 2)$.*

5.3 Embedding dimension

We shall now address the problem of the choice of the embedding dimension d, which was considered as fixed in the above discussion. For a generic time series $\{x_j\}$, $j = 1, ..., K$, we consider embedding spaces whose dimension is related to the number K of points available. For example, if $K = 1000$ we let d vary between 2 and 8, according to the *fundamental limitation* provided in Eckmann and Ruelle (1992). When a deterministic case is detected its embedding dimension is computed as the value at which the curves $\lambda_k(r_0)$ against r_0 are straight and parallel lines as the iteration parameter k is varied. However, we want to stress that in order to reconstruct the attractor's dynamics it might be necessary to embed the trajectory in a space whose dimension is greater than the *true* dimension of the state space (compare with Eckmann *et al.*, 1986).

6 Applications

Discrete time series may be derived from mappings, continuous systems (taking the discretisation over finite times) or experimental data. With explicit dynamical systems, the time series is formed by the iterations of one observable, typically one of the system's coordinate. We consider several examples of low-dimensional mappings and apply the method to characterise the deterministic system, compute the Lyapunov exponents and compare the results with the classical numerical ones (see Section 6.1). Continuous systems are analysed in Section 6.2 and analyses of experimental data derived from neurobiology (precisely, from the epochs of action potentials in electro-physiological recordings) are presented in Section 6.3. Validation of the method by considering surrogate data and simulated spike trains is presented in Section 6.4.

6.1 Mappings

Below is a list of dissipative mappings and the corresponding tables reporting the values of the LCE (λ_1) and its classical numerical estimate (λ_C) for several choices of the parameters of the mappings. In all cases the time series was constructed as the iterates of the x-component with $K = 1000$ points and λ_1 was calculated for $r_0 = r_{\max}$. We refer to Celletti *et al.* (1999) for a more extensive discussion of the 2-dimensional Hénon mapping and of the Rössler system.

6.1.1 Hénon mapping (2-dimensional)

It is defined by the equations

$$\begin{aligned} x' &= -ax^2 + y + 1 \\ y' &= bx \ , \end{aligned}$$

$x, y \in \mathbf{R}$ and $a, b \in \mathbf{R}$. Let λ_C be the classical numerical estimate of the LCE and λ_1 be the value obtained as in Section 5, with an embedding dimension $d = 2$; let x_0, y_0 be the initial conditions.

x_0	y_0	a	b	λ_C	λ_1 $(d=2)$
0.6	0.19	1.6	0.1	0.352	0.325
0.5	0.20	1.6	0.1	0.354	0.311
0.4	0.10	1.4	0.15	0.349	0.331

6.1.2 Hénon mapping (4-dimensional)

It is defined by the equations

$$\begin{aligned} x' &= -ax^2 + y + 1 \\ y' &= bx + hz\ , \\ z' &= -a'z^2 + t + 1\ , \\ t' &= -b'z + hx\ , \end{aligned}$$

x, y, z, $t \in \mathbf{R}$ and a, b, a', b', $h \in \mathbf{R}$. We adopt the same notations as before for λ_C and λ_1.

x_0	y_0	z_0	t_0	a	b	a'	b'	h	λ_C	λ_1 $(d=4)$
0.6	0.19	0.62	0.192	1.4	0.3	1.6	0.6	0.01	0.405	0.378
0.6	0.19	0.62	0.192	1.4	0.3	1.6	0.6	0.001	0.420	0.380
0.6	0.19	0.62	0.192	1.4	0.3	1.6	0.6	0.03	0.400	0.363
0.6	0.19	0.62	0.192	1.6	0.2	1.2	0.1	0.001	0.440	0.460
0.6	0.19	0.62	0.192	1.6	0.2	1.2	0.1	0.005	0.440	0.474
0.5	0.21	0.82	0.4	1.6	0.2	1.2	0.1	0.001	0.440	0.493
0.5	0.21	0.82	0.4	1.6	0.2	1.2	0.1	0.005	0.441	0.468
0.62	0.18	0.62	0.19	1.6	0.2	1.2	0.1	0.001	0.440	0.465
0.62	0.18	0.62	0.19	1.4	0.31	1.61	0.6	0.01	0.430	0.394
0.62	0.18	0.62	0.19	1.4	0.31	1.61	0.6	0.001	0.423	0.371

6.1.3 Kaplan–Yorke map

It is defined by the equations

$$\begin{aligned} x' &= ax \qquad\qquad (\mathrm{mod}\ 1) \\ y' &= \alpha y + b\cos(2c\pi x)\ , \end{aligned}$$

x, $y \in \mathbf{R}$, a, b, c, $\alpha \in \mathbf{R}$. In a 2-dimensional embedding space, for any initial conditions we have the following results.

a	b	c	α	λ_C	λ_1 $(d=2)$
3	2	1	0.2	1.099	1.164
3	2	1	0.25	1.099	1.164
3	2	1	0.5	1.099	1.164

6.1.4 Zaslavskii map

It is defined by the equations

$$\begin{aligned} x' &= x + v(1+\mu y) + \varepsilon v \mu \cos x \qquad \pmod{2\pi} \\ y' &= e^{-\gamma}(y + \varepsilon \cos x) , \end{aligned}$$

where x, $y \in \mathbf{R}$ and the parameters are real numbers with

$$\mu = (1 - e^{-\gamma})/\gamma$$

$$v = (4/3) \cdot 100.$$

Taking the initial conditions $x_0 = y_0 = 0$, we have the following results.

ε	γ	λ_C	λ_1 $(d=2)$
0.1	3	0.758	0.683
0.15	3	1.278	1.324
0.3	3	1.928	1.773
0.2	2	1.426	1.468
0.2	4	1.358	1.347
0.3	4	1.922	1.765
0.4	4	2.158	1.931

6.1.5 Ikeda map

Let

$$z' = p + B\, z\, e^{ik - i\alpha/(1+|z|^2)} , \tag{3}$$

where $z \in \mathbf{C}$ and p, B, k, $\alpha \in \mathbf{R}$. We rewrite (3) in its real form as

$$\begin{aligned} x' &= p + B\cos(k - \frac{\alpha}{1+x^2+y^2})\ x - B\sin(k - \frac{\alpha}{1+x^2+y^2})\ y \\ y' &= \qquad B\cos(k - \frac{\alpha}{1+x^2+y^2})\ y + B\sin(k - \frac{\alpha}{1+x^2+y^2})\ x \end{aligned}$$

and take $k = 0.4$. In this example, the best λ_1 is always obtained in a 3-dimensional embedding space. For comparison, we report also the value corresponding to $d = 2$.

x_0	y_0	p	B	α	λ_C	$\lambda_1(d=3)$	$\lambda_1(d=2)$
0.1	0.5	1	0.9	6	0.507	0.488	1.092
0.1	0.1	1	0.9	6	0.507	0.410	1.030
0.1	0.1	1	0.9	6.5	0.487	0.443	1.178
0.1	0.1	0.9	0.9	6	0.420	0.382	0.943
0.1	0.1	1.1	0.8	6	0.466	0.454	0.800

6.1.6 Sinai map

$$\begin{aligned} x' &= x + y + \Delta \cos(2\pi y) \qquad && (\text{mod } 1) \\ y' &= x + y && (\text{mod } 1)\ , \end{aligned}$$

where x, $y \in \mathbf{R}$, $\Delta \in \mathbf{R}$. We take $x_0 = y_0 = 0.1$; the correct value of λ_1 is in some cases obtained taking a higher dimensional embedding space.

Δ	λ_C	$\lambda_1(d=3)$	$\lambda_1(d=2)$
0.1	0.687	0.555	0.638
0.3	0.614	0.705	1.080
0.01	0.693	0.661	0.577
0.005	0.693	0.706	0.644
0.12	0.685	0.617	0.758
0.15	0.681	0.612	0.993

6.2 Continuous systems

For continuous systems the 1000 points time series are derived from the x' iterates of the discretised x-component, when integrating by, e.g., a Runge-Kutta method. The experimental time series x'' were constructed by taking the series formed by the intervals $x''_i = x'_{i+1} - x'_i$. The resolution of the time series generated from the regular dynamics of conservative systems should be carefully taken into account. In the present study the experimental time series x'' were arbitrarily scaled in such a way that $x''_{\text{max}} = 100000$, which represents a very high resolution. For comparison with the electro-physiological *spike trains* the series generated out of the continuous systems were characterised by a pseudo 'firing rate' of 0.1 spikes/s.

We have tested our method for three continuous systems whose data were contaminated by various levels of noise . In particular, we show the results of the effect of 5% additive, dynamical and experimental noise. For continuous systems, the computation of the LCE definitely requires more than 1000 points. However, we show that the method is still able to detect the deterministic behaviour when data series of length $K = 1000$ are considered.

6.2.1 Lorenz system (3-dimensional)

It is defined by the equations

$$\begin{aligned} \dot{x} &= \sigma(y - x) \\ \dot{y} &= x(R - z) - y \\ \dot{z} &= xy - bz \end{aligned}$$

Figure 6 shows the curves $\lambda_k(r_0)$ as functions of the initial distance r_0 (for $k = 1, ..., 5$) for the parameters $\sigma = 16$, $R = 45.92$, $b = 4$. In Figure 6(a) the application of our method to the plain time series indicates that the curves tend to become parallel and flat. Conversely, for 5% additive, dynamical and experimental noise, Figures 6(b), 6(c) and 6(d) respectively, show that curves are not parallel. We tested the *Lorenz system* also for two other choices of parameters, namely for $\sigma = 10$, $R = 28$, $b = 8/3$ and for $\sigma = 16$, $R = 40$, $b = 4$. In both such cases our method differentiated the plain time series from the 5% noisy series.

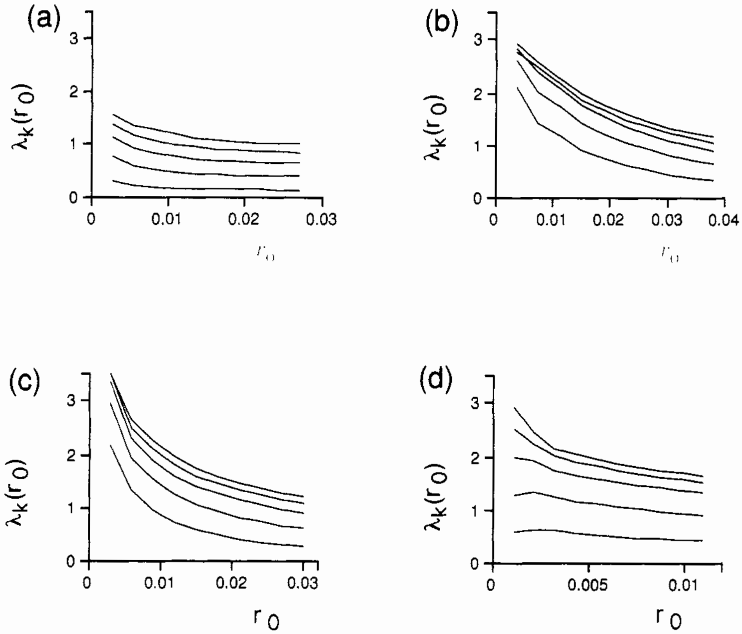

Figure 6. *The Lorenz system embedded in a 3-dimensional space is considered for the parameters* $\sigma = 16$, $R = 45.92$, $b = 4$. *(a) The graphs refer to the curves* $\lambda_k(r_0)$ *against* r_0 *as* $k = 1, ..., 5$ *for a 1000 points time series. (b) Analysis of the original time series with* 5% *additive noise; (c)* 5% *dynamical noise; (d)* 5% *experimental noise.*

6.2.2 Rössler system (3-dimensional)

It is defined by the equations

$$\begin{aligned} \dot{x} &= -y - z \\ \dot{y} &= x + ay \\ \dot{z} &= b + z(x - c) \end{aligned}$$

Figure 7 shows the curves $\lambda_k(r_0)$ against r_0 as $k = 1, ..., 5$ for the parameters $a = 0.2$, $b = 0.2$ and $c = 10$ for the plain, 5% additive, dynamical and experimental noisy time series. We tested the *Rössler system* also for the following choices of parameters: $a = 0.2$, $b = 0.4$, $c = 5.7$; $a = 0.2$, $b = 0.2$, $c = 5.7$; $a = 0.15$, $b = 0.2$, $c = 10$. In all cases the plot of $\lambda_k(r_0)$ against r_0 allowed to discriminate plain series from 5% noisy series.

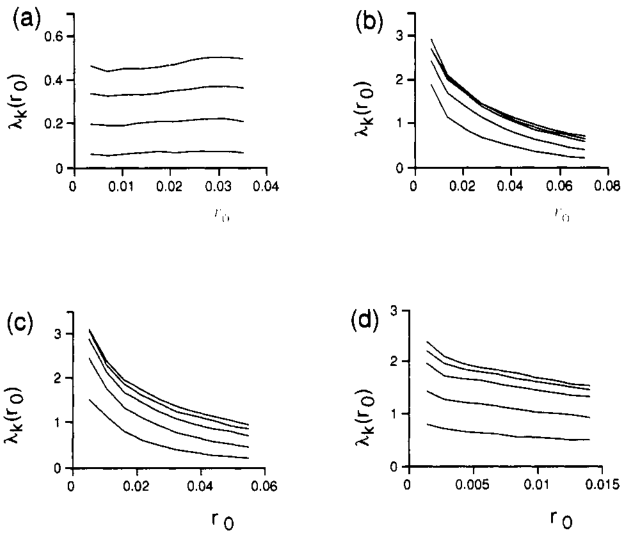

Figure 7. *The Rössler system in a 3-dimensional space is considered for the parameters $a = 0.2$, $b = 0.2$, $c = 10$. (a) The graphs refer to the curves $\lambda_k(r_0)$ against r_0 as $k = 1, ..., 5$ for a 1000 points time series. (b) Analysis of the original time series with 5% additive noise; (c) 5% dynamical noise; (d) 5% experimental noise.*

6.2.3 Hyperchaotic Rössler system (4-dimensional)

It is defined by the equations

$$\begin{aligned} \dot{x} &= -y - z \\ \dot{y} &= x + ay + w \\ \dot{z} &= b + xz \\ \dot{w} &= cw - dz , \end{aligned}$$

We considered this system for the parameters $a = 0.25$, $b = 0.3$, $c = 0.05$, $d = 0.5$. Figure 8 shows the curves $\lambda_k(r_0)$ against r_0 as $k = 1, ..., 5$ for the plain, 5% additive, dynamical and experimental noisy time series.

6.3 Neuro-biological data

The basic frequency of a neuron is usually in the range 1–5 Hz, allowing the neuron to be ready to transmit information. When excited, the frequency of the neuron may increase up to 50 Hz, sometimes even up to 500 Hz for few a milliseconds. Let $\{t_j\}$ be the sequence of *firing times* of a given neuron. We analysed several data sets collected during neuro-biological experiments under different recording conditions. All experiments were performed in compliance with the guidelines for the care and use of laboratory animals edited by the Society of Neuroscience and after receiving governmental veterinary approval. Extracellular single unit recordings were made with glass-coated tungsten microelectrodes having an impedance in the range 0.5–2 $M\Omega$ measured at a frequency of 1kHz.

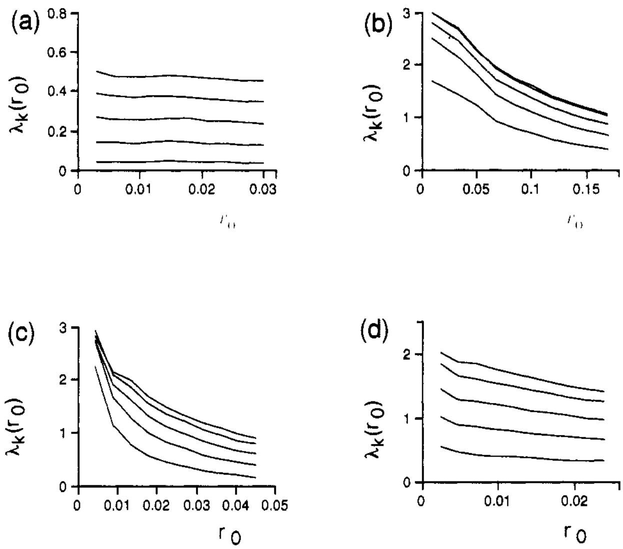

Figure 8. *The hyperchaotic Rössler system in a 4-dimensional space is considered for the parameters* $a = 0.25$, $b = 0.3$, $c = 0.05$, $d = 0.5$. *(a) The graphs refer to the curves* $\lambda_k(r_0)$ *against* r_0 *as* $k = 1, ..., 5$ *for a 1000 points time series. (b) Analysis of the original time series with* 5% *additive noise; (c)* 5% *dynamical noise; (d)* 5% *experimental noise.*

All recordings were stationary as it pertains to the normal electro-physiological criteria. The firing times $\{t_j\}$ of the nervous cells were stored digitally for off-line analysis. The *spike train* is provided by the discrete time series formed by consecutive intervals of firing, i.e. $\{x_1, ..., x_j, ..., x_K\} \equiv \{t_1 - t_0, ..., t_j - t_{j-1}, ..., t_K - t_{K-1}\}$, where the experiments are performed up to time t_K. We considered only time series with a minimum of 800 points.

The dynamics of 214 spike trains recorded in the temporal cortex of anesthetised mice (Schwaller *et al.*, 1998) were investigated by using both the GP method and the method of Section 5. The firing rate of these cells extended over the range 0.43–1.99 spikes/s. The accuracy of the time epochs was set to 1 ms. Note that the temporal cortex receives inputs from the auditory system and is connected to other sensory and associative cortical areas. The anaesthetic condition was maintained in a steady state throughout the recording session. The data analysed here concern only those periods of time when no external stimuli was applied (so-called 'spontaneous activity', labelled as *sp*). Up to ten blocks of 100 seconds each were cumulated for the analysis of single spike trains.

Another set of data consisted in 139 spike trains recorded in the red nucleus neurons of conscious freely moving rats while they performed a simple forelimb reaching movement with the contralateral forepaw. This nucleus is an important centre of the motor system. The data were provided by Brian Hyland at the Department of Physiology, University of Otago, New Zealand. The firing rate of these neurons varied between 7.5 and 43.2 spikes/s. The accuracy of spikes timing was set to 0.1 ms, thus providing a comparable resolution with the other data set described above. The relationship of activity changes in these neurons to phase of task performance is reported elsewhere (Hyland and Jarratt, 1999). Data were recorded continually while the animals repeatedly reached for, grasped, and then consumed small pieces of food. For analysis, data were segmented into 2 sets thus providing 278 time series. Each set made up of multiple blocks of 4 seconds each. One set, referred to as *mvt*, included the 2 seconds before and after each occasion the food was grasped, and so included the acts of reaching, grasping, and withdrawing of the food. The other set was made up of blocks taken from periods between reaching episodes and is referred to as a control period *(ctl)*.

Spike train	*Rec*	K	d	d_{GP}	D_2
$m2agc2.12\_A$	sp	921	4	4	1.50
$m1ahc1.13\_3$	sp	1073	5	5	0.92
$m1bac2.12\_B$	sp	1050	5	5	1.66
$m1bdc6.09\_4$	sp	2567	4	4	0.28
$rn01c6\_1.A11$	ctl	1037	6	5	3.80
$rn22c08.A2$	ctl	1248	5	4	3.40
$rn18c07.A11$	ctl	1441	5	4	0.46
$rn04c05.A1$	ctl	1941	5	4	2.05
$rn29c08.A1$	ctl	1083	4	4	1.39
$rn07c07.A11$	mvt	1050	4	4	0.31
$rn08c08.A2$	mvt	2072	4	4	2.60

By using the GP method we found 13/214 and 21/278 spike trains which exhibited a chaotic attractor in the mice temporal cortex and the rat red nucleus, respectively. Our method confirmed that 11/34 cases do show clear features of deterministic systems embedded in a low-dimensional space. These results are reported in Table I, where *Rec* indicates the recording condition, K denotes the total number of points, d is the embedding dimension at which the series are deterministic according to our algorithm, d_{GP} and D_2 are the embedding and correlation dimensions as provided by the GP method. Figure 9 illustrates one experimental case of deterministic dynamics observed in the red nucleus of freely moving rats during the control period.

6.4 Surrogate data

The method was tested on several sets of *surrogate* data derived from the original discrete time series. We considered the time series as point processes, i.e. $\{x_j\} \equiv \{t_j\}$. The intervals between two consecutive points $\{t_j - t_{j-1}\}$ were randomly shuffled. In such a way the first-order statistics (i.e., the time interval histogram) remained unchanged but the dynamics was completely scrambled. This construction of surrogate time series was applied to deterministic mappings, continuous systems and experimental data. In addition, to test the method on simulated spike trains we created surrogate data according to Abeles and Gerstein (1988) as realisations of non-stationary Poisson processes at different firing rates and different rates of fluctuations. We examined about 200 surrogate data sets with $K = 1000$ points and we always found that the LCE curves were not parallel, not straight lines, no matter what the embedding dimension was (up to $d = 8$).

In a few cases we noticed that the application of the GP method to simulated spike

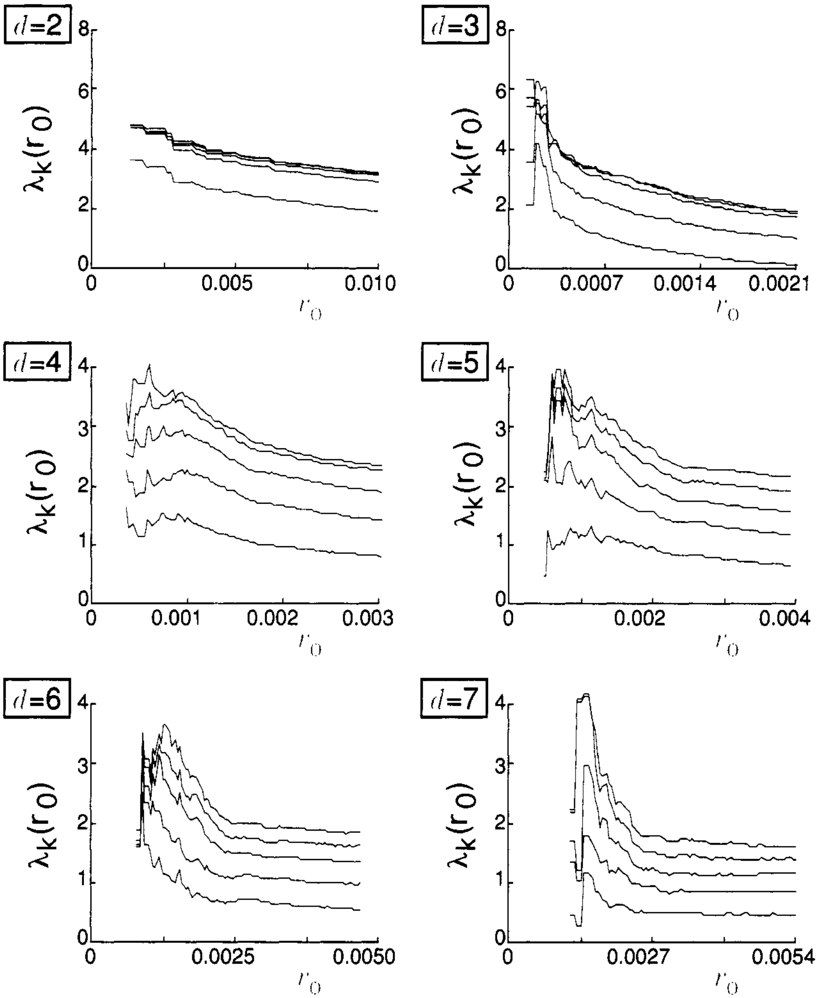

Figure 9. *A neuro-biological application is considered. The example refers to the spike train rn18c07.A11 and includes 1441 points. The curves $\lambda_k(r_0)$ against r_0 are shown as $k = 1, ..., 5$ and for embedding dimensions $d = 2, ..., 7$. A deterministic behaviour is observed for an embedding dimension $d \geq 5$.*

trains could suggest a deterministic behaviour, even if all spike intervals were generated by chance. Figure 10 illustrates the analysis of a spike train generated according to a non-stationary Poisson distribution with fast fluctuation (0.05 s) of firing rate (Tetko and Villa, 1997). The average firing rate was 3.7 spikes/s and it fluctuated in range of 0–54 spikes/s. The application of our algorithm did not detect any deterministic behaviour for all analysed embedding dimensions. However, such behaviour was detected by the GP method.

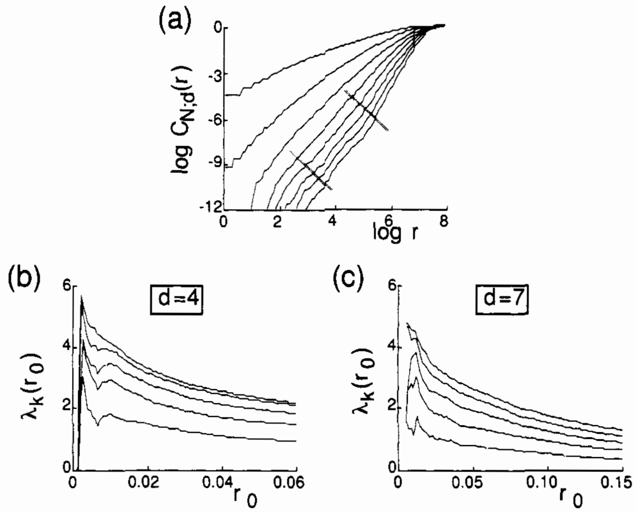

Figure 10. *Dynamical system analysis of a simulated spike train generated by non-stationary Poisson distribution. (a) The GP algorithm detects deterministic behaviour with $d_{\rm GP} = 4$, $D_2 = 2.08$. The scaling region is enhanced by grey lines. The curves $\lambda_k(r_0)$ against r_0 are plotted for $k = 1, \ldots, 5$ within an embedding space of dimension $d = 4$ in (b) and dimension $d = 7$ in (c). Note that no deterministic behaviour is observed.*

7 Other methods for short time series

The method presented in Section 5 works properly in many dynamical situations, particularly when dealing with chaotic regimes of conservative mappings and when analysing dissipative systems. However, some dynamics of conservative mappings cannot be satisfactorily investigated with the method of Section 5. Precisely, for the analysis of regular orbits and of weak chaotic motions, one needs to apply slightly different techniques as provided in (Lega *et al.*, 2000).

Recalling the notations of Section 5, let $\alpha_{ij}^{(k)} \equiv \log \frac{d_{i,j}^{(k)}}{d_{i,j}^{(0)}}$. Let $\widehat{\lambda}_k$ be the average of $\alpha_{ij}^{(k)}$ over the $(N-k)$ pairs of nearest neighbours having distances $d_{i,j}^{(0)}$ $(N \doteq K - d + 1)$:

$$\widehat{\lambda}_k = \frac{1}{(N-k)} \sum_{\{i=1,\ldots,N-k;\ j:d_{i,j}^{(0)} = \min_{\bar{j}} d_{i,\bar{j}}^{(0)}\}} \alpha_{ij}^{(k)} \,. \tag{4}$$

The LCE is provided by $\widehat{\lambda}_1$ or equivalently by $\widehat{\lambda}_k/k$. A *mixed method* which results as a compromise between (1) and (4) can be obtained as follows. For each point P_j locate its nearest neighbour P_i. Order the distances $d_{i,j}^{(0)}$ between nearest neighbours from the smallest to the largest and consider only the first h pairs of nearest neighbours. In Lega *et al.* (2000) the first $h = (N-k)/10$ pairs were considered in order to cover the orbit as much as possible and to have small initial distance vectors. Consider the images $P_i^{(k)}$ and $P_j^{(k)}$ after k iterations until their distance $d_{i,j}^{(k)}$ becomes greater than a given threshold r_0.

Let $k(P_i, P_j)$ be the time necessary for $d_{i,j}^{(0)}$ to become greater than the threshold r_0. Excluding the pairs whose initial distance is greater than r_0, define

$$\alpha_{i,j}^{k(P_i,P_j)} \equiv \log \frac{d_{i,j}^{k(P_i,P_j)}}{d_{i,j}^{(0)}}$$

and call $\widetilde{\lambda}(r_0)$ the average over the $h = (N - k)/10$ first pairs of nearest neighbours (renumbered from 1 to h) having distances $d_{i,j}^{k(P_i,P_j)} > r_0$ after $k(P_i, P_j)$ iterations:

$$\widetilde{\lambda}(r_0) = \frac{1}{h} \sum_{\{i=1,\ldots,h;\ j:d_{i,j}^{(0)}=\min_{\tilde{j}} d_{i,\tilde{j}}^{(0)}\}} \frac{\alpha_{ij}^{k(P_i,P_j)}}{k(P_i,P_j)}\,. \tag{5}$$

The Lyapunov exponents as computed using (1), (2), (4), (5) were compared in Lega *et al.* (2000) for the 2-dimensional Hénon's map and for the standard mapping described by the equations

$$\begin{aligned} x_{i+1} &= x_i + \epsilon \sin(x_i + y_i) && \mod (2\pi) \\ y_{i+1} &= x_i + y_i && \mod (2\pi). \end{aligned}$$

Several dynamical behaviour of the standard map were investigated (circulation torus, libration island, weak chaos, chaos, strong chaos). In all cases (both dissipative and conservative), the mixed (Equation 5) provides the best result when compared to the other methods. With the speed of computation, it is wise to use all algorithms to cross-check the results.

8 Discussion

In Celletti *et al.* (1999) we presented a new algorithm to test for low-dimensional determinism of a short time series and to provide a good estimate of the maximum Lyapunov exponent (LCE) based on the measure suggested in Boffetta *et al.* (1998), Cellucci *et al.* (1997), Gao and Zheng (1993), Kantz (1994). The method depends only on two *free* parameters: the iteration parameter and the initial distance. In Section 5, we have provided simple arguments for the choice of these parameters and performed a χ^2-test on some mathematical models to validate these criteria. We have applied the method of Celletti *et al.* to many discrete systems, showing that it is able to discriminate correctly the deterministic behaviour of the time series. Also in the case of continuous systems, our method correctly detects the deterministic dynamics. Our method of discretising these systems was aimed at providing time series with comparable resolution to experiment. Then, we have arbitrarily scaled the values in order to obtain point processes with characteristics similar to those observed in spike trains, namely an average rate of 0.1–5.0 spikes/s at a resolution of 1ms; the LCE curves showed a stable behaviour over this range. Surrogate data were also considered and in all cases a stochastic behaviour was found.

As a concrete application of the method presented in Section 5, we considered experimental time series derived from neuro-biological studies. In this case, time series are usually short and are characterised by noise variances of 10% or more of the signal variance (Rapp 1993, Theiler and Rapp 1996). The test for determinism of such series, in particular for the analysis of time series derived from brain activity such as extracellular single unit spike trains, has often been put in doubt because of the limited possibility to discriminate low levels of noise offered by established methods of analysis. To this respect, a method based on the measure of Gao and Zheng (Gao and Zheng, 1993) has been recently developed (Cellucci *et al.*, 1997) to detect noise in time series derived from Rössler, Lorenz and Mackey–Glass attractors with more than 8000 points. The problem of estimating the effect of noise corruption in time series data is difficult (Schreiber and Kantz, 1996) and depends on the nature of noise, either observational or dynamical (Theiler *et al.*, 1992). To this end, we considered the effect of additive, dynamical and experimental noise and compared our algorithm to the method developed by Grassberger and Procaccia (Grassberger and Procaccia, 1983). Without applying any noise filtering technique the noisy time series was identified as deterministic by the GP method, but not by our method. This result indicates a high level of sensitivity to noise by our technique. However, the GP method has the advantage of providing information on the dimensions of the embedding and of the attractor, if any, and was successfully used in studies of neuro-biological data (Babloyantz and Salazar 1985, Celletti and Villa 1996, Mpitsos *et al.* 1988, Rapp *et al.* 1985). Therefore, we would suggest the application of the GP method at first in order to discriminate the candidate time series for deterministic dynamics. On these selected series, the complementary use of our method would provide a more precise evaluation of which data may follow a strict deterministic behaviour.

The finding of strict deterministic dynamics in several spike trains investigated in this study confirms the previous results obtained by applying the GP method (Babloyantz and Salazar 1985, Celletti and Villa 1996, Mpitsos *et al.* 1988, Rapp *et al.* 1985). These results establish the existence in the brain of some mechanisms able to support stable nonlinear dynamics of neuronal firing over a time that must be suitable to process some meaningful information in the brain. Theoretical prediction of the existence of such attractor networks was suggested in relation to representation of learned stimuli and was simulated in large scale neural networks with simple but reasonable assumptions of interactions between neurons (e.g., Amit and Brunel 1997, Herrmann *et al.* 1993). We may raise the hypothesis that a number of neuronal networks, each one being potentially described by a limited set of differential equations (given the low-dimensionality in the experimental findings), may interact at the level of selected single-units. Therefore, the analysis of deterministic dynamics in the brain might provide a new measure of the level of interacting networks at different conditions, encompassing also clinical and pharmacological manipulations. The method adopted in this work is simple enough to be implemented in an efficient computer program and could be used as a complementary method to the routinely accepted time domain analyses of spike trains.

Acknowledgments

We are grateful to B. Hyland for many discussions during the accomplishment of this work and for providing us with experimental data. We thank G. Della Penna and E. Lega for helping us in the numerical computation of the Lyapunov exponents. A. Celletti was partially sponsored by GNFM (Gruppo Nazionale per la Fisica Matematica); A. Villa and I. Tetko were partially supported by Swiss National Science Foundation grant #2150–045689.95 and INTAS-OPEN grant #97–0168 grants.

References

Abarbanel H D I, 1996, *Analysis of observed chaotic data*, New York: Institute for Nonlinear Science, Springer-Verlag

Abarbanel H D I, Brown R, Sidorowich J J and Tsimring L S, 1993, *Rev Mod Phys* **65**, 1331.

Abeles M and Gerstein G L, 1988, *J Neurophysiol* **60**, 909.

Amit D J and Brunel N, 1997, *Cerebral Cortex* **7**, 237.

Babloyantz A and Salazar J M, 1985, *Phys Lett A* **111**, 152.

Benettin G and Galgani L, 1979, "Lyapunov characteristic exponents and Stochasticity, Intrinsic Stochasticity in plasma" in *Les éditions de Physique*, ed G Laval and D Gresillon (Coutaboeuf Orsay - France)

Benettin G, Galgani L, Giorgilli A and Strelcyn J M , 1980, *Meccanica* **15**, 9.

Boffetta G, Crisanti A, Paparella F, Provenzale A and Vulpiani A, 1998, *Physica* **116D**, 301.

Celletti A, Bajo V and Villa A E P, 1998, *Meccanica* **33**, 381.

Celletti A, Froeschlé C, Tetko I V and Villa A E P, 1999, *Meccanica* **252**, 1.

Celletti A and Villa A E P, 1996, *Biological Cybernetics* **74**, n. 5, 387.

Cellucci C J, Albano A M, Rapp P E, Pittenger R A and Josiassen R C, 1997, *Chaos* **7**, 414.

Dämming M and Mitschke F, 1993, *Phys Lett* **178**, 385.

Eckmann J P, Kamphorst Oliffson S, Ruelle D and Ciliberto S, 1986, *Phys Rev A* **34**, 4971.

Eckmann J P and Ruelle D, 1985, *Rev Mod Phys* **57**, 617.

Eckmann J P and Ruelle D, 1992, *Physica* **56D**, 185.

Froeschlé C, 1984, *Cel Mech* **34**, 95.

Gao J and Zheng Z, 1993, *Phys Letters A* **181**, 153.

Grassberger P and Procaccia I, 1983, *Phys Rev A* **28**, 2591.

Hegger R, Kantz H and Schreiber T, 1999, *Chaos* **9**, n. 2, 413.

Herrmann M, Ruppin E and Usher M, 1993, *Biol Cybern* **68**, 455.

Hyland B I and Jarratt H, 1999, *Neuroscience* **88**, 629.

Kantz H, 1994, *Phys Lett A* **185**, 77.

Kaplan D T and Glass L, 1992, *Phys Rev Lett* **68**, n. 4, 427.

Lega E, Celletti A, Della Penna G and Froeschlé C, 2000, to appear in *Int J Bif and Chaos*

Mpitsos G J, Burton R M Jr, Creech H C and Soinila S O, 1988, *Brain Res Bull* **21**, 529.

Packard N H, Crutchfield J P, Farmer J D and Shaw R S, 1980, *Phys Rev Lett* **45**, 712.

Rapp P E, 1993, *The Biologist* **40**, 89.

Rapp P E, Albano A M, Schmah T I and Farwell L A, 1993, *Phys Rev* **47E**, 2289.

Rapp P E, Zimmerman I D, Albano A M, Deguzman G C and Greenbaun N N, 1985, *Phys Lett A* **110**, 335.

Rosenstein M T, Collins J J and de Luca C J, 1993, *Physica* **65D**, 117.

Schreiber T, 1998, *Phys Rep* **308**, 1.

Schreiber T and Kantz H, 1996, "Observing and Predicting chaotic signals: Is 2% noise too much?" in *Predictability of Complex Dynamical Systems*, ed Y A Kravtsv and J B Kadtke **69**, 43, Springer Series in Synergetics.

Schwaller B, Villa A E P, Tetko I V, Hunziker W, Tandon P, Silveira D C and Celio M, 1998, *Europ J Neurosci Suppl* **10**, 4.

Sugihara G and May R M, 1990, *Nature* **344**, 734.

Tetko I V and Villa A E P, 1997, *Biol Cybern* **76**, 397.

Theiler J, Eubank S, Longtin A, Galdrikian B and Farmer J D, 1992, *Physica* **58D**, 77.

Theiler J and Rapp P E, 1996, *Electroenceph Clin Neurophysiol* **98**, 213.

Wolf A, Swift J B, Swinney H L and Vastano J A, 1985, *Physica* **16D**, 285.

Zeng X, Eykholt R and Pielke R A, 1991, *Phys Rev Lett* **66**, 3229.